Supplemental Discussion and Figures
for "A spurious jump in the satellite record: Is Antarctic sea ice really expanding?"

S1 Detailed description of data and methods

Here we discuss the ice concentration fields analyzed in this study and the resulting time series of ice extent and ice area that we calculate.

S1.1 Ice concentration

The ice concentration datasets considered in this study are derived from passive microwave measurements from instruments flown on a series of satellites. The Scanning Multichannel Microwave Radiometer (SMMR) was flown on the NASA Nimbus 7 satellite and provided data between 26 October 1978 and 20 August 1987, with the Bootstrap sea ice concentration using the data between 1 November 1978 and 31 July 1987. SMMR measured radiances in 10 channels including 18.0H, 18.0V, 21.0V, 37.0H, and 37.0V; here the number refers to the frequency in GHz and the letter indicates vertical (V) or horizontal (H) polarization. Although the Nimbus 7 passed over both polar regions every day, the radiometer operated only on alternate days due to power limitations, leading to a temporal resolution of 2 days. SMMR was succeeded by the Special Sensor Microwave/Imager (SSM/I), which measured radiances every day in 7 channels including 19.3H, 19.3V, 22.2V, 37.0H, and 37.0V. SSM/I instruments were flown on a sequence of three Department of Defense satellites beginning in July 1987, and the Bootstrap sea ice concentration uses data during 1 August 1987 until 13 December 2007 with transitions between satellites occurring on 3 December 1991 and 1 October 1995. The Special Sensor Microwave Imager Sounder (SSMIS), which measures radiances in 24 different channels including 19.3H, 19.3V, 22.2V, 37.0H, and 37.0V, has been generating daily data from a Department of Defense satellite since 14 December 2006, with the Bootstrap sea ice concentration using data starting on 1 August 2008.

We consider both hemispheres in this Supplement. We focus on ice concentration datasets generated from the passive microwave radiance measurements using the Bootstrap algorithm, and in this Supplement we also consider data generated with the NASA Team algorithm. The Bootstrap algorithm uses data from the 19V, 37V, and 37H channels, and the NASA Team algorithm uses data from the 19H, 19V, and 37V channels. Both algorithms also draw on the 22V channel to filter out weather effects. The use of brightness temperature ratios in the NASA Team algorithm reduces errors due to surface temperature variations, but unlike the Bootstrap algorithm, the NASA Team algorithm is biased toward underestimating sea ice concentrations (Comiso et al., 1997). Both algorithms have empirically adjusted parameters that differ between the two hemispheres, and the parameters in the Bootstrap algorithm also vary on a daily basis.

Various steps go into processing the ice concentration data to inter-calibrate across the transition from one sensor to another and to fill in missing or identifiably erroneous pixels. Although a number of brief data gaps exist, the instruments have provided data for at least 20 days of every month (10 days for SMMR) from November 1978 to present with the exception of December 1987 and January 1988, when the SSM/I instrument was turned off between 3 December 1987 and 13 January 1988 due to overheating issues.

The effective resolution (sensor footprint) of the microwave measurements vary as a function of frequency, with the resolution of the most coarse frequency used by the Bootstrap and NASA Team algorithms being approximately 40 km $\times$ 70 km. However, all concentrations are derived from daily average passive microwave brightness temperatures mapped onto a polar stereographic grid with a nominal resolution of 25 $\times$ 25 km.

A region around each pole is not imaged due to the inclination angle of the satellite orbit. This hole is located poleward of 84.5°N for SMMR and 87.2°N for SSM/I and SSMIS.

The Bootstrap data is processed at NASA Goddard Space Flight Center and distributed by NSIDC (Comiso, 2000), and we acquired from NSIDC the daily Bootstrap ice concentration datasets from before (Version 1) and after (Version 2) the entire dataset was reprocessed in September 2007 using the updated Bootstrap algorithm from Comiso and Nishio (2008).

S1.2 Ice extent and ice area

We calculate the daily ice area in a given hemisphere from the gridded ice concentration field in both Bootstrap versions by summing the area of each pixel weighted by the ice concentration. Following a standard convention (e.g., Cavalieri et al., 1999), we exclude pixels with ice concentration less than 15% due to wind roughening and other weather filtering issues near the ice edge.

A more common measure of the hemispheric sea ice cover is the ice extent, which is defined as the area of all pixels with ice concentration above a specified threshold, normally taken to be 15% since this has been found to correspond with the ice edge estimated using aircraft measurements (Cavalieri et al., 1991). We calculate the daily ice extent for both Bootstrap versions following this convention, and ice extent is used exclusively in the main paper. An advantage of using ice extent rather than ice area is that ice extent is less sensitive to errors in the ice concentration field, such as those associated with the misidentification of surface melt ponds during the summer as open ocean. Two disadvantages of using ice extent is that it is less physically relevant, since it includes the area of patches of open water within the ice pack, and that it depends more on pixel resolution.

In the Arctic, we mask lakes from the ice concentration field and assume the hole around the pole has 100% ice concentration; note that this causes a small erroneous decrease in Arctic sea ice area in 1987 associated with the decrease in the radius of the hole between SMMR and SSM/I.

We compute daily ice extent and then take monthly averages, rather than computing the ice extent from monthly averaged ice concentration fields, which avoids biases associated with the merging of temporal and spatial averages. We average the ice extent and ice area over all days in each month with data, with the exception of December 1987 and January 1988, when there was limited data as described above. These two months are filled using linear interpolation between the same month in the previous year and the following year. The result is a monthly time series of ice extent and ice area for each Bootstrap version in each hemisphere.

The Version 1 dataset that we were able to acquire from NSIDC ends in December 2004, whereas the dataset considered in the IPCC AR4 (Solomon et al., 2007) continued through the end of 2005. Hence for the comparison in Fig. 1B with the trend reported in the IPCC AR4, we electronically lifted the annual ice extent from Fig. 4.8 of the IPCC AR4 and use this data to extend the Version 1 data in Fig. 1B (red solid line) by one year: the trend from years 1979–2004 and 1979–2005 of the AR4 annual ice extent data is included in Fig. 1B as points above December 2004 and December 2005, respectively, connected by a red dashed line.

For the NASA Team algorithm, we use a time series of monthly-mean ice extent and ice area downloaded from the NSIDC "Sea Ice Index" archive (Fetterer et al., 2002). We interpolate over the months 12/1987 and 1/1988, as we do for the Bootstrap algorithm, and we add the area of the hole around the pole to the Arctic sea ice area.

The three time series of monthly-mean ice extent and ice area in both hemispheres all begin in November 1978, but they end at different times. The Bootstrap Version 1 dataset ends in December 2004, the Bootstrap Version 2 dataset ends in December 2012, and the NASA Team dataset ends in August 2013 (including Near-Real-Time data during the months of 2013 because final NASA Team data was not yet available).

S1.3 Documented update to Bootstrap algorithm

A separate satellite passive microwave dataset is available from the Advanced Microwave Scanning Radiometer for the Earth Observing System (AMSR-E), which is flown on the NASA Aqua satellite. AMSR-E provided data from 19 June 2002 until 4 October 2011, when an antenna problem caused the sensor to stop operating. Compared to SSM/I, AMSR-E has finer spatial resolution and provides data over a wider range of microwave frequencies.

The transition from SSM/I to AMSR-E sea ice concentration in some multi-instrument datasets was found previously to lead to an artificial increase in the Antarctic sea ice area (Screen, 2011). Note that this study does not include AMSR-E sea ice data.

The Bootstrap algorithm was revised and a new version of the NASA Team algorithm (NASA Team 2) was created for use with the AMSR-E data (Comiso et al., 2003). Considering four years of overlap between AMSR-E and SSM/I (2002-2006), ice covers estimated with the Bootstrap algorithm from both satellites, as well as NASA Team SSM/I results, were all found to be in fairly good agreement overall for both hemispheres (Comiso and Parkinson, 2008; Parkinson and Comiso, 2008). Comiso and Nishio (2008), however, identified a small bias between ice cover data estimated from AMSR-E and SSM/I measurements using the Bootstrap algorithm. An adjustment was made to the Bootstrap dataset for consistency between the two instruments, after which Comiso and Nishio (2008) found that the 1978–2006 record that had AMSR-E data during 2002–2006 had a trend of 10.8×10^3 km^2 per year, nearly identical to the 1978–2006 trend in the original SMMR and SSM/I Bootstrap dataset which they found to be 10.9×10^3 km^2 per year.

S2 Structure of trends in both hemispheres

Here we examine further details of the sea ice trends that are not included in the main paper. We examine ice area as well as ice extent. For comparison with the two Bootstrap versions, we consider ice cover estimated using the NASA Team algorithm. We also consider the ice extent and ice area from the same three datasets in the Arctic.

S2.1 Monthly ice extent and ice area

We focus on anomalies from the mean seasonal cycle in each record (Fig. S1). The difference between the two Bootstrap versions and the NASA Team ice extent is plotted in Fig. S2B,C in order to see whether it allows us to discern which of the two Bootstrap versions had an erroneous offset inserted or removed in December 1991. However, the differences between the NASA Team record and each version of the Bootstrap record are too large and noisy to isolate any readily discernible change around December 1991.

The difference in ice area between Bootstrap Version 2 and Version 1 similarly shows a transition in December 1991 (Fig. S2D). But for ice area, as for ice extent, the difference between each Bootstrap version and the NASA Team data is too large and variable to discern which Bootstrap dataset experienced the jump (Fig. S2E,F): there is no step around December 1991 that stands out above the month-to-month variability, even though a difference in trend is apparent in some panels (Figs. 2A,B,D,F).

Because similar algorithms are used in both hemispheres, we also consider ice extent and ice area anomalies in the Arctic (Fig. S3). For the Arctic sea ice extent, a persistent offset appears to be introduced between the two records at the sensor change in August 1987. The NASA Team ice extent drops considerably below both Bootstrap versions around this sensor change (Fig. S4B), causing a spike in the comparison with either Bootstrap version (Fig. S4B,C). The Arctic sea ice area shows similar features, although the difference between the Bootstrap datasets is less impacted by the August 1987 sensor change. Note that compared with both Bootstrap versions, the NASA Team ice extent has a substantial spike at the October 1995 sensor change, and the NASA Team ice area has a similar spike at the August 1987 sensor change, although our analysis does not discern whether this is due to an error in the NASA Team data or in both versions of the Bootstrap data. Overall, we do not see a compelling indication in the Arctic ice extent or ice area data whether Bootstrap Version 1 or Version 2 is more likely to contain errors in both hemispheres.

S2.2 Ice extent and ice area trends

We examine the trend in the Bootstrap Version 1 and Version 2 data, as well as the NASA Team data, in both hemispheres. It is instructive to compare the differences between the datasets with the reported error bar on the trend, which provides an indication of the significance of the jump in trend between Version 1 and Version 2. Ice extent trends are often reported with error bars based on the 68% linear regression confidence interval (e.g., Comiso and Steffen, 2001; Comiso, 2003; Comiso and Nishio, 2008; Comiso, 2010), which is an estimate of the error associated with natural variability about the trend. Note that the IPCC AR4 and IPCC AR5 instead use a 90% linear regression confidence interval (see Appendix A1 of main text).

In the Antarctic, the Bootstrap Version 2 ice extent trend is well outside the 68% confidence interval of the Bootstrap Version 1 trend and near the edge of the 99.7% confidence interval for all plotted record endpoints in Fig. S5B. Similar features apply to the trend in sea ice area: the trend in Bootstrap Version 2 is above the 95% confidence interval of the Bootstrap Version 1 trend (Fig. S5E).

The trend in the Bootstrap Version 2 ice extent (Fig. S5A) agrees fairly closely with the NASA Team data (Fig. S5C), whereas Bootstrap Version 1 does not (Fig. S5B), implying that an error in the Bootstrap dataset may have been corrected between Version 1 and Version 2. In contrast, however, the trend in NASA Team ice area (Fig. S5F) agrees closely with Bootstrap Version 1 (Fig. S5E) but not with Bootstrap Version 2 (Fig. S5A), implying instead that Version 2 introduced an error into the Bootstrap dataset that did not exist in Version 1. This could be related to the previously discussed low bias in NASA Team ice concentration (e.g., Comiso et al., 1997), which could plausibly affect the ice area trend.

However, the comparison is reversed in the Arctic. The trend in Arctic sea ice area agrees closely between both Bootstrap versions and NASA Team, whereas the trend in Arctic sea ice extent differs substantially between each of the three records (Fig. S6). Interestingly, the trend in Bootstrap Version 2 Arctic sea ice extent falls near the edge of the 99.7% regression confidence interval of the NASA Team trend (Fig. S6C): If both current datasets are seen as reliable estimates of the sea ice cover, then this indicates that the regression confidence interval substantially underestimates the uncertainty in the Arctic sea ice trend by failing to account for errors associated with the ice concentration retrieval.

In the Arctic, the trend in sea ice extent differs between Version 1 and Version 2 (Fig. S6), leading to a spurious jump in the reported trend as for the Antarctic. However, in contrast to the Antarctic, this jump is relatively small compared with the physical changes in the linear trend during the past decade, i.e., the acceleration of the ice retreat.

S2.3 Seasonal structure of trends

There is not a strong seasonal structure to the trend in the Antarctic sea ice cover in any of the datasets considered here (Fig. S7). Although the trend is larger in March/June than in September/December for many record endpoints in all three ice extent datasets, both Bootstrap Version 2 and NASA Team produce trends that are smallest in March for the most recent record endpoints. Other studies that have reported the trend to be largest in Austral summer have measured the trend in percent per decade, dividing the trend by the mean value for each month and thereby introducing a strong seasonality associated with the denominator (e.g., Turner and Overland, 2009).

The seasonal uniformity in the Antarctic is in contrast with the Arctic (Fig. S8), where the retreat is fastest in boreal late summer, a feature that has been attributed to the configuration of continents in the Arctic (Eisenman, 2010).

S2.4 Spatial structure of trends

The spatial structure of the trends in both Bootstrap versions is compared in Fig. S9. We consider the change between the late 1980s and the late 1990s in order to focus on the shift that occurred in December 1991 (Fig. 2). Both versions have nearly identical spatial patterns of the change for all seasons during this time period. In most locations and seasons, Version 2 changes in a more positive way than Version 1 during this period. The difference between the two versions is relatively uniform spatially and among seasons (lowest row in Fig. S9), in contrast with the strongly spatially-varied trend in each dataset individually and consistent with a sensor calibration issue explaining the difference between the versions.

References

Cavalieri, D. J., Crawford, J. P., Drinkwater, M. R., Eppler, D. T., Farmer, L. D., Jentz, R. R., and Wackerman, C. C.: Aircraft active and passive microwave validation of sea ice concentration from the defense meteorological satellite program special sensor microwave imager, J. Geophys. Res., 96, 21 989–22 008, doi:10.1029/91JC02335, 1991.

Cavalieri, D. J., Parkinson, C. L., Gloersen, P., Comiso, J. C., and Zwally, H. J.: Deriving long-term time series of sea ice cover from satellite passive-microwave multisensor data sets, J. Geophys. Res., 104, 15 803–15 814, doi:10.1029/1999JC900081, 1999.

Comiso, J.: Bootstrap Sea Ice Concentrations from Nimbus-7 SMMR and DMSP SSM/I-SSMIS. Version 2, Boulder, CO, USA: National Snow and Ice Data Center, (Updated 2012.) http://nsidc.org/data/nsidc-0079.html, 2000.

Comiso, J. C.: Large Scale Characteristics and Variability of the Global Sea Ice Cover, in: Sea Ice–An Introduction to its Physics, Biology, Chemistry and Geology, pp. 112–142, Blackwell Scientific Ltd, 2003.

Comiso, J. C.: Variability and Trends of the Global Sea Ice Cover, in: Sea Ice, pp. 205–246, Wiley-Blackwell, 2nd edn., 2010.

Comiso, J. C. and Nishio, F.: Trends in the sea ice cover using enhanced and compatible AMSR-E, SSM/I, and SMMR data, J. Geophys. Res., 113, C02S07, doi:10.1029/2007JC004257, 2008.

Comiso, J. C. and Parkinson, C. L.: Arctic sea ice parameters from AMSR-E data using two techniques and comparisons with sea ice from SSM/I, J. Geophys. Res., 113, C02S05, doi:10.1029/2007JC004255, 2008.

Comiso, J. C. and Steffen, K.: Studies of Antarctic sea ice concentrations from satellite data and their applications, J. Geophys. Res., 106, 31 361–31 385, doi:10.1029/2001JC000823, 2001.

Comiso, J. C., Cavalieri, D. J., Parkinson, C. L., and Gloersen, P.: Passive microwave algorithms for sea ice concentration: A comparison of two techniques, Remote Sens. Environ., 60, 357–384, 1997.

Comiso, J. C., Cavalieri, D. J., and Markus, T.: Sea ice concentration, ice temperature, and snow depth using AMSR-E data, IEEE Transactions On Geoscience Remote Sensing, 41, 243–252, doi:10.1109/TGRS.2002.808317, 2003.

Eisenman, I.: Geographic muting of changes in the Arctic sea ice cover, Geophys. Res. Lett., 37, L16 501, doi:10.1029/2010GL043741, 2010.

Fetterer, F., Knowles, K., Meier, W., and Savoie, M.: Sea ice index, Natl. Snow and Ice Data Cent., Boulder, Colo., (Updated 2012.) http://nsidc.org/data/g02135.html, 2002.

Parkinson, C. L. and Comiso, J. C.: Antarctic sea ice parameters from AMSR-E data using two techniques and comparisons with sea ice from SSM/I, J. Geophys. Res., 113, C02S06, doi:10.1029/2007JC004253, 2008.

Screen, J. A.: Sudden increase in Antarctic sea ice: Fact or artifact?, Geophys. Res. Lett., 38, L13 702, doi:10.1029/2011GL047553, 2011.

Solomon, S., Qin, D., Manning, M., Chen, Z., Marquis, M., Averytand, K., Tignor, M., and Miller, H., eds.: Climate Change 2007: The Physical Science Basis. Contribution of Working Group I to the Fourth Assessment Report of the Intergovernmental Panel on Climate Change, Cambridge University Press, Cambridge, UK, 2007.

Turner, J. and Overland, J.: Contrasting climate change in the two polar regions, Polar Res., 28, 146–164, doi:10.1111/j.1751-8369.2009.00128.x, 2009.

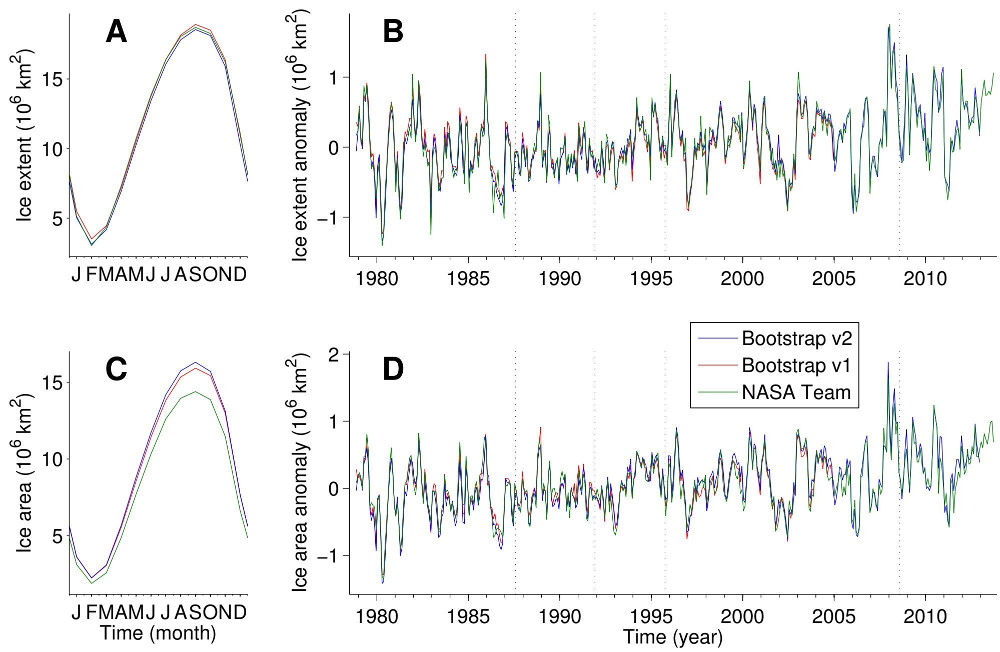

Fig. S1. (A) Mean seasonal cycle of Antarctic sea ice extent during 1979-2004 and (B) time series of monthly-mean anomalies from the mean seasonal cycle for both versions of the Bootstrap data as well as the NASA Team data. (C)-(D) Same, but for ice area rather than ice extent.

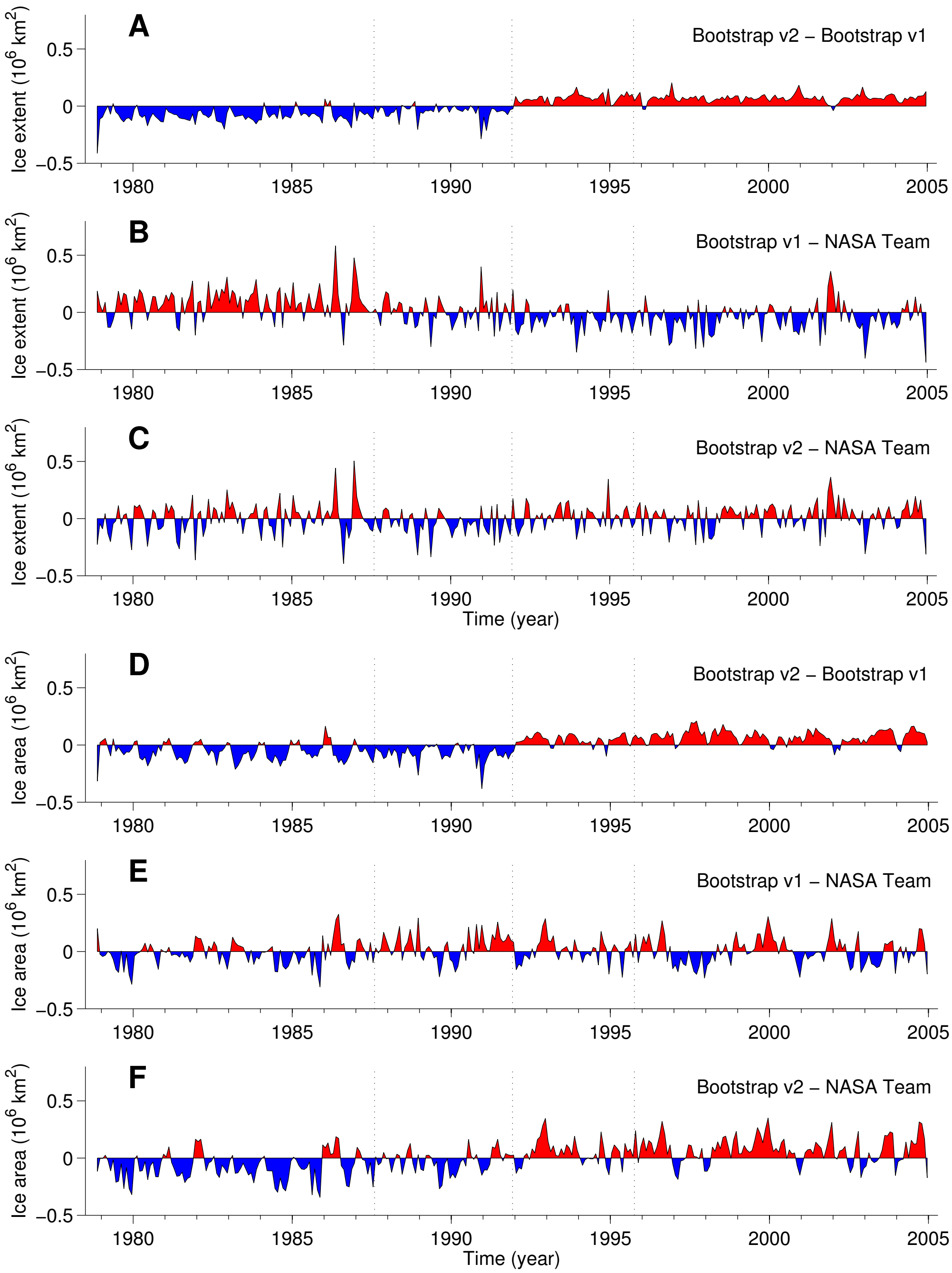

Fig. S2. Antarctic sea ice anomalies from the mean seasonal cycle. (A-C) Difference between monthly-mean Antarctic sea ice extents computed using Bootstrap Version 1, Bootstrap Version 2, and NASA Team algorithms. Datasets are indicated in the top right corner of each panel. Panel A is equivalent to Fig. 2. (D-F) Same, but for ice area rather than ice extent. Transitions between sensors are indicated by vertical dotted lines (see Sec. S1.1). The plotted time interval is the period during which Bootstrap Version 1 data is available.

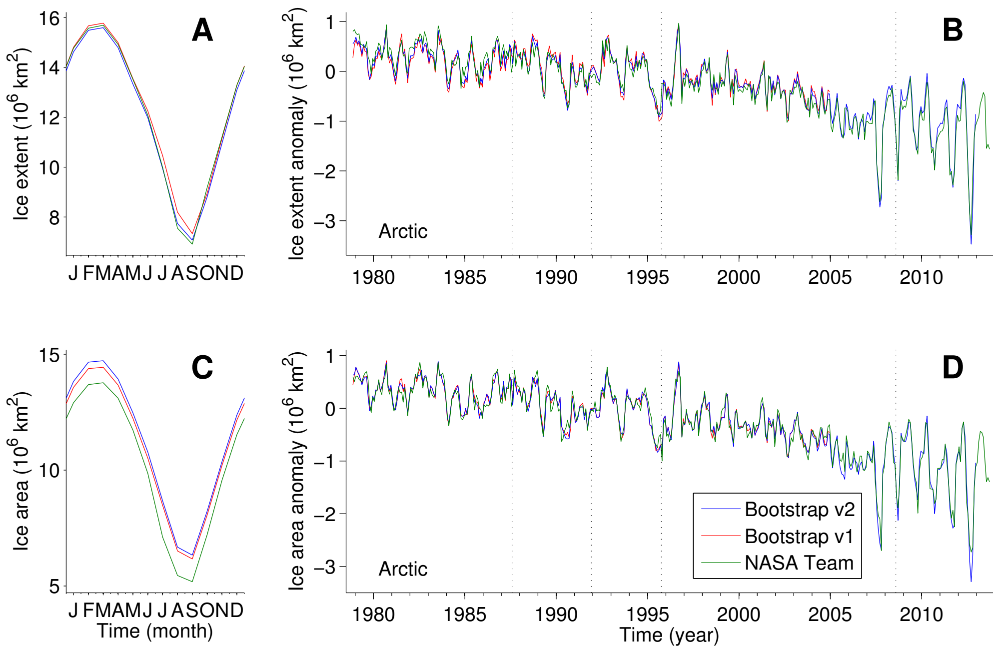

Fig. S3. As in Fig. S1, but for the Arctic.

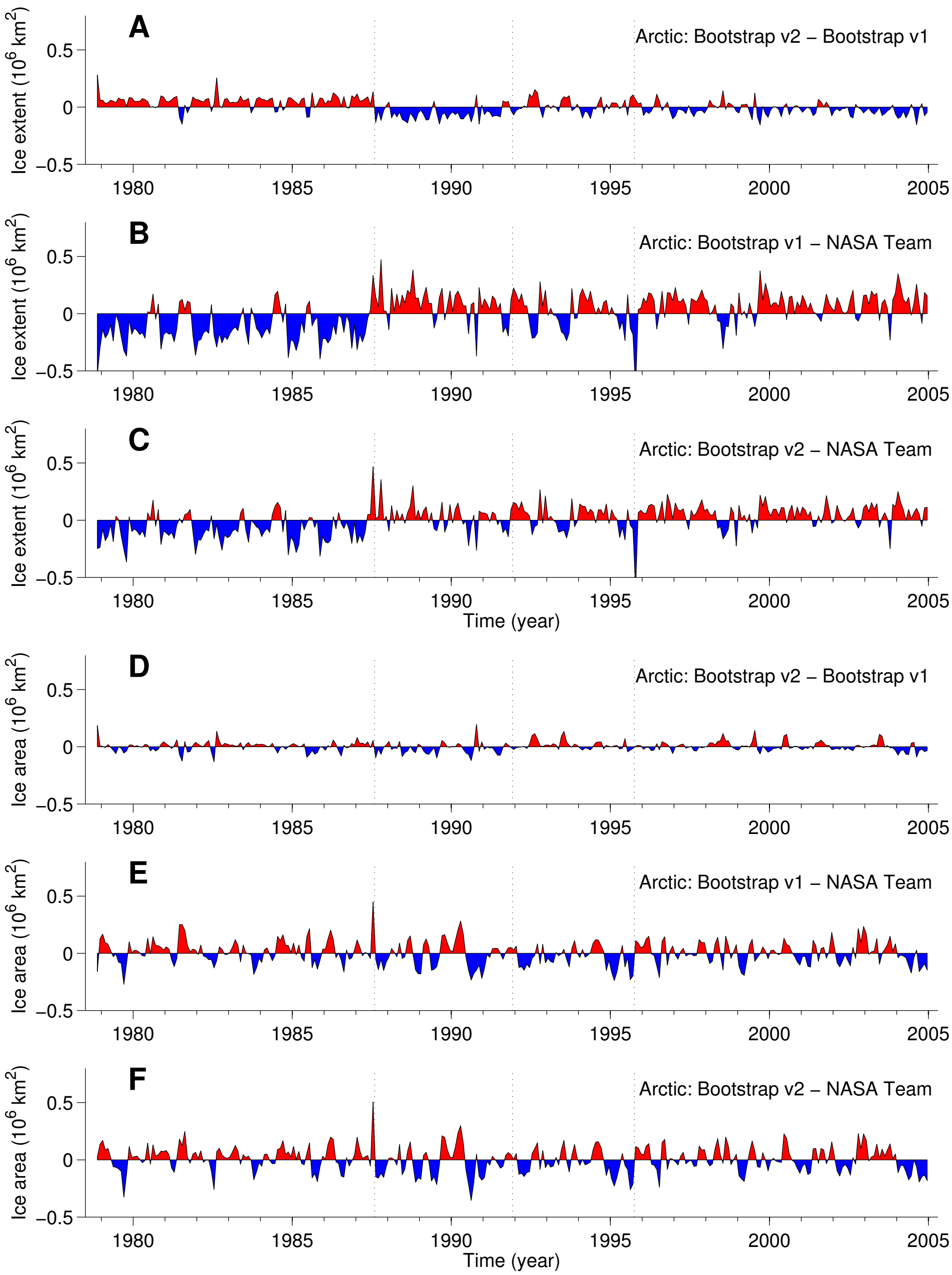

Fig. S4. As in Fig. S2, but for the Arctic.

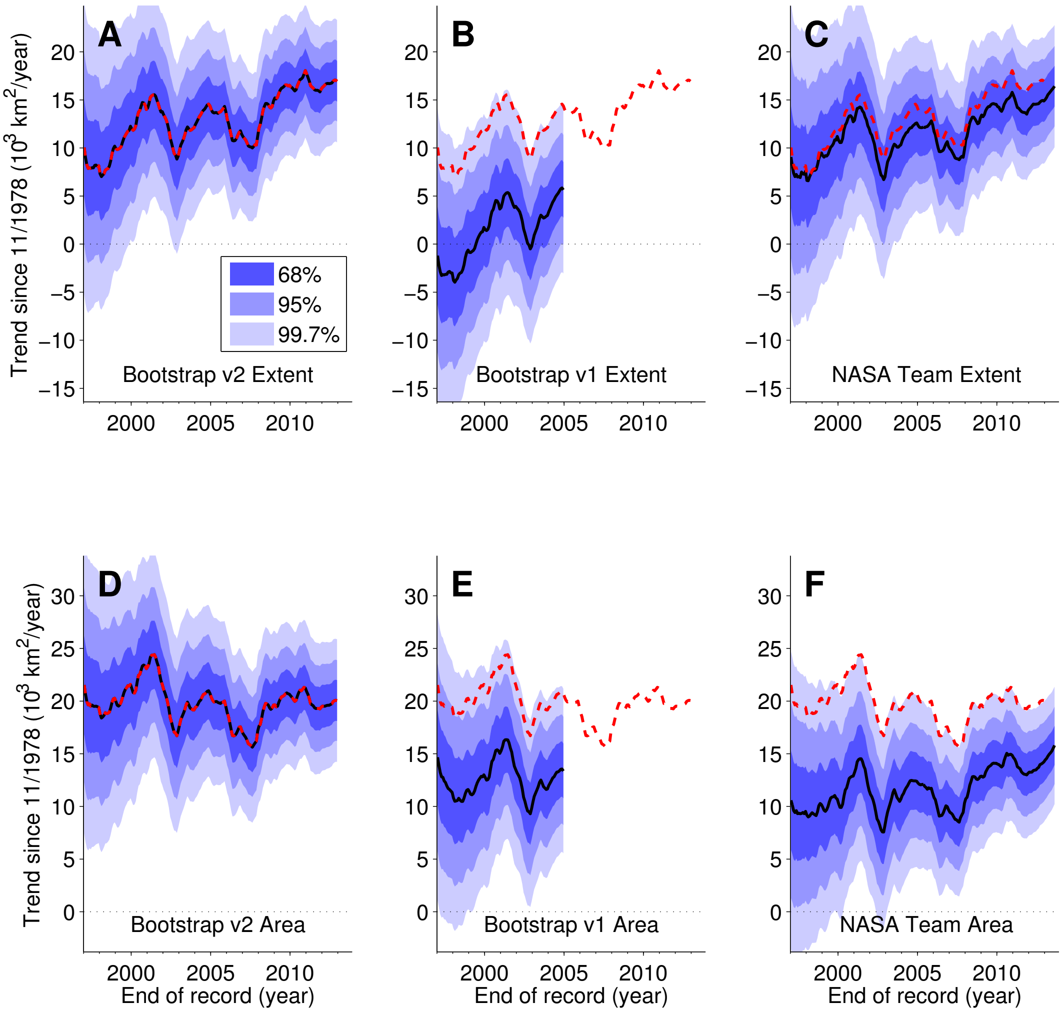

Fig. S5. Trends for Antarctic sea ice extent (top) and area (bottom) using Version 1 and Version 2 of the Bootstrap algorithm, as well as the NASA Team algorithm, as a function of the record end date. Dark blue shading indicates the 68% regression confidence interval, which is often used to represent the trend error bar; 95% and 99.7% confidence intervals are also indicated. The trend computed using Version 2 of the Bootstrap algorithm (red dashed line) is repeated across each row for comparison.

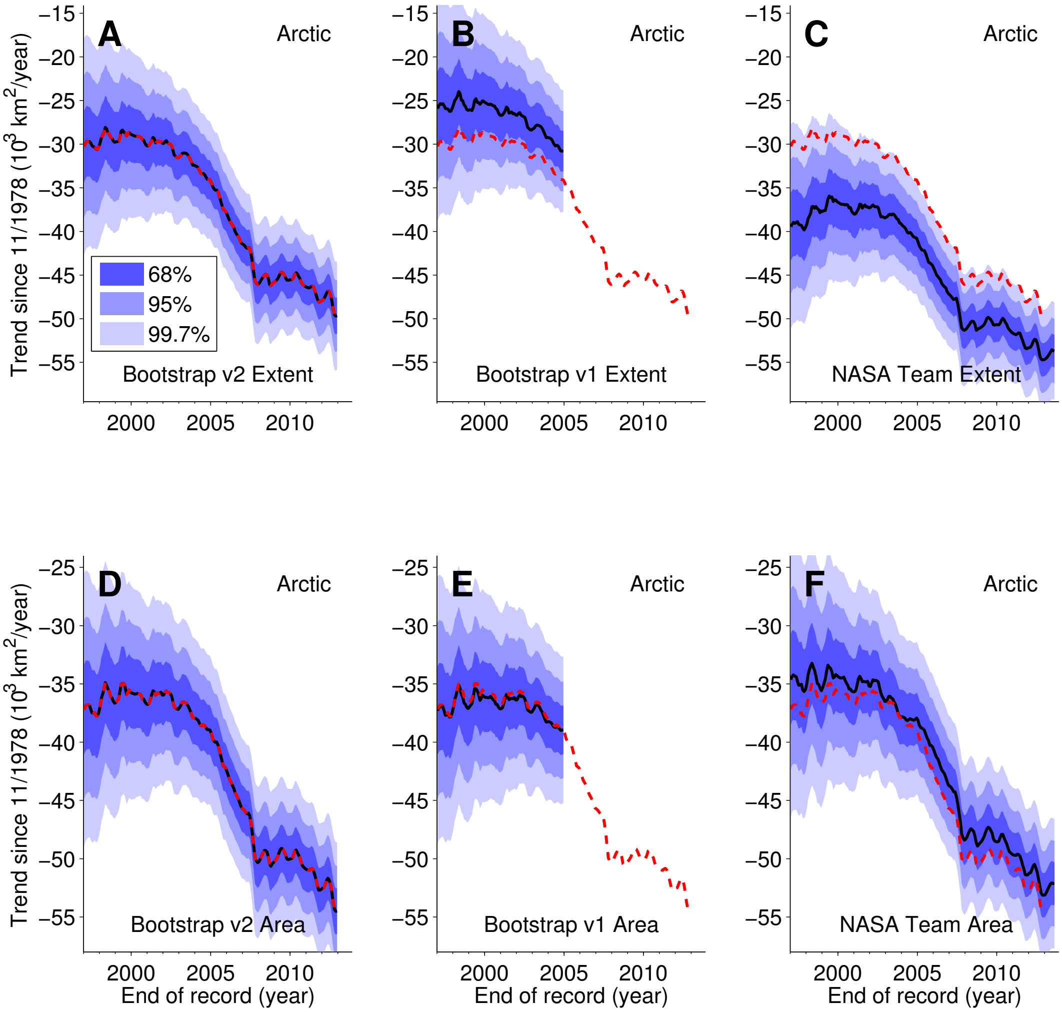

Fig. S6. As in Fig. S5, but for the Arctic.

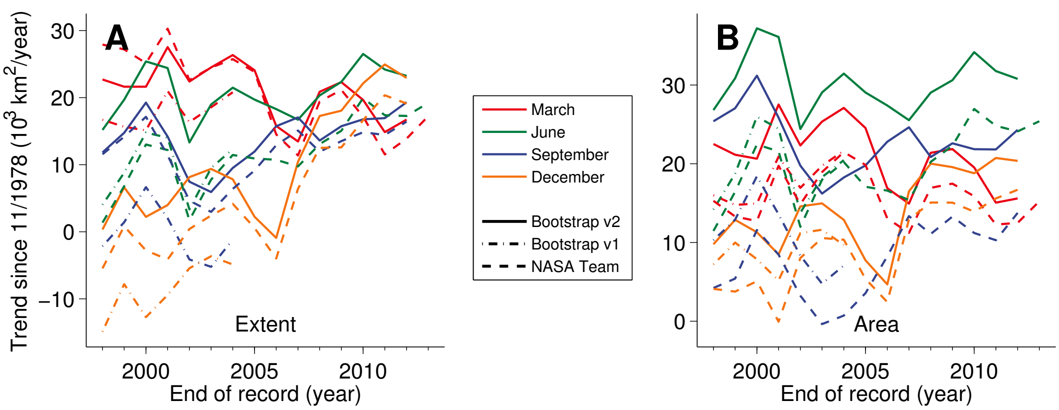

Fig. S7. Seasonal structure of trends in Antarctic (A) ice extent and (B) ice area. Here the trends are computed using only every March (red), June (green), September (blue), or December (orange) as a function of the record end date. Results are plotted for Version 2 of the Bootstrap algorithm (solid), Version 1 of the Bootstrap algorithm (dot-dash), and the NASA Team algorithm (dash).

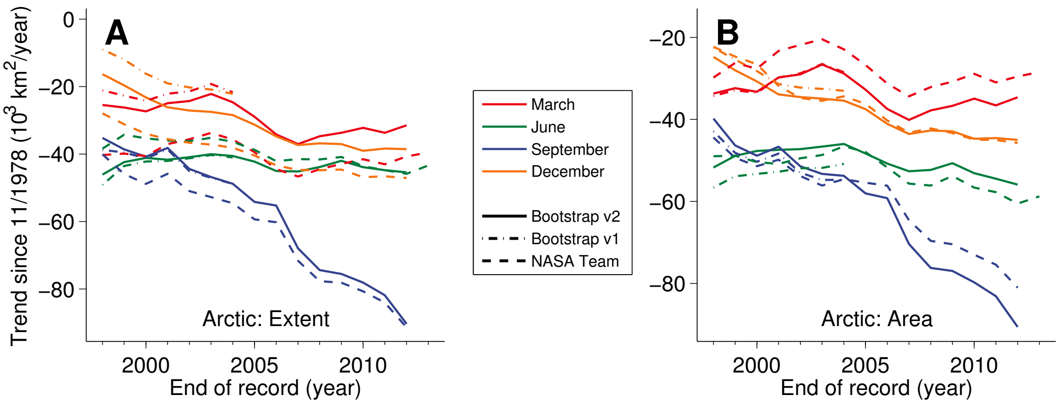

Fig. S8. As in Fig. S7, but for the Arctic.

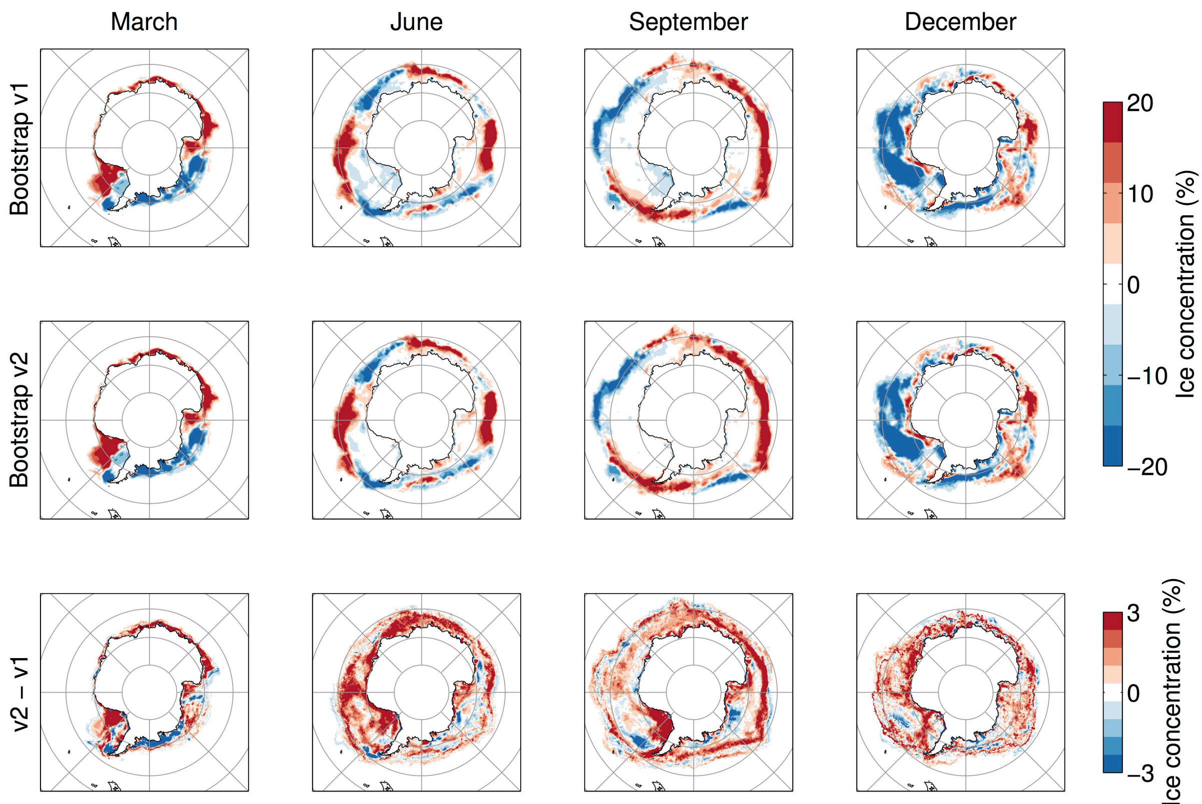

Fig. S9. Spatial structure of changes in Antarctic sea ice cover. (Top row) Change between late 1980s and late 1990s, calculated as the mean during 1985–1989 subtracted from the mean during 1995–1999, in Bootstrap Version 1 dataset. (Middle row) Same, but for Bootstrap Version 2 dataset. (Bottom row) Difference between Bootstrap versions, calculated as Version 2 minus Version 1. Each column represents a different month.